Coupled gravimetric, manometric and calorimetric study of CO_2, N_2 and CH_4 adsorption on zeolites for the assessment of classical equilibrium models

Alejandro Orsikowsky-Sanchez[1,2] · Frédéric Plantier[2] · Christelle Miqueu[2]

Abstract

N_2, CO_2 and CH_4 pure gas adsorption equilibria on five zeolites with different structural properties (Si/Al ratio, type of cations contained inside their structure, pore size and pore volume) have been measured over a wide range of pressures (from 10^{-5} to 80 bar) and temperatures (from 253 to 363 K) by combining high pressure gravimetric technique and high resolution low pressure manometry. These experimental data, coupled with the measurement of the differential heat of adsorption and with some literature information obtained with microscopic studies, have allowed to identify and to analyze the different adsorption mechanisms. The results show that CO_2 adsorption mechanism is controlled by molecule–cation interactions at low pressures and by the pore volume filling at intermediate and high pressures. On the contrary, N_2 and CH_4 adsorption mechanism is controlled by the pore volume filling in the whole range of pressures studied in this work. It is shown that the most popular models used in gas separation modeling such as Toth, Sips and bi-Langmuir do not describe the successive physico-chemical phenomena observed for the adsorption of CO_2 on zeolites. Moreover, they are not able both to fit the whole range of experimental data and to predict the isosteric heat of adsorption accurately.

Keywords Adsorption isotherm · Zeolites · Differential heat of adsorption · Adsorption modeling

1 Introduction

Natural gas processing requires complex separation and purification operations involving expensive CAPEX (Capital Costs) and OPEX (Operational Costs) processes. The separation of CO_2 is performed using adsorption, absorption or membranes strategies, for which significant expenses can arise related to the removal of impurities. In the case of low to moderate levels of impurities, adsorption processes may be economically preferable. Current research on anthropogenic CO_2 capture also highlights many adsorbents (Cheung and Hedin 2014; Wang et al. 2014; Tagliabue et al. 2009). Given the large number of adsorbents developed and cited in the literature for natural gas treatment or CO_2 capture, industry is facing with the problem of sorting the most promising adsorbents. Within these adsorbents, zeolites appear to be potential very good candidates because of their low cost, thermal and mechanical stability and their microporous nature (Gleichmann et al. 2016). LTA, FAU and MFI zeolites are widely studied in the frame of gas separation by adsorption (Hefti et al. 2015; Mofarahi and Gholipour 2014; Gholipour and Mofarahi 2016; Harlick and Tezel 2003).

The standard evaluation of adsorbents for gas separation involves both the measurement and the modeling of pure gases and mixtures adsorption together with dynamic behavior tests such as breakthrough curves before simulating the industrial processes. In general, the modeling of adsorption properties is carried out using simple macroscopic models (such as Toth, Sips and bi-Langmuir) whose implementation in the process simulation softwares is simple (Yang 1999).

✉ Alejandro Orsikowsky-Sanchez
  alejandro.orsikowsky@total.com

✉ Christelle Miqueu
  christelle.miqueu@univ-pau.fr

1 TOTAL EP – Pôle d'Etudes et de Recherche de Lacq (PERL), BP 64170, Lacq, France

2 CNRS/TOTAL/UNIV PAU & PAYS ADOUR, Laboratoire Des Fluides Complexes Et Leurs Réservoirs - IPRA, UMR5150, 64600 Anglet, France

The estimation of the adsorption properties at equilibrium conditions is the essential starting point for a correct representation and evaluation of storage and separation processes. Hence, it is crucial to understand the limitations of these most popular thermodynamic models used for the modeling of gas separation by adsorption.

The aim of this work is twofold. First, a combined gravimetric, manometric and calorimetric investigation of CO_2, N_2 and CH_4 adsorption on five commercial zeolites with different properties (Si/Al ratio, type of cation, pore size and pore volume) is performed over a wide range of pressures and temperatures. Then, this new complete database is used in combination with structural microscopic information in order to identify the adsorption mechanisms and to assess the classical adsorption models—such as Toth, Sips and bi-Langmuir—used in the modeling of gas separation by adsorption processes.

2 Experimental section

2.1 Materials

Five commercial pure zeolite powders have been selected according to different criteria. Thereby, the selected zeolites allow to analyze different structures and the factors influencing the adsorption mechanisms such as the Si/Al ratio, the type of cation, the pore size and the pore volume (Bonenfant et al. 2008). All zeolite samples were provided by Fisher Scientific.

Table 1 shows the different selected zeolites, the type of structure, the Si/Al ratio, the type of cation and the theoretical values of pore size (Baerlocher et al. 2007; Ruthven 1984).

The FAU pseudo-structure consists of a tetrahedral network composed of sodalite cages linked to each other by rings with six oxygen atoms (D6R). This assembly contains a large central cage with a diameter of nearly 13 Å. The windows that give access to the central cages (pore opening) have a diameter of about 7.4 Å. The sodalite cages—because they are linked by D6R rings whose size is very small—are not accessible to the different molecules. The accessible pore structure of this three-dimensional structure is composed of the highly interconnected central cages. The LTA pseudo-structure consists of eight β cages (or sodalite cages) located at the corners of a cube and connected by rings composed of four oxygen atoms (D4R). This assembly gives rise to a large polyhedral central cage (α cage) with a diameter of approximately 11.4 Å. The stacking of this units in a cubic network creates three-dimensional structure where cages are connected by windows. The passage section through the window varies, depending on the type and the mobility of the cations present in the structure, giving rise to different types of LTA zeolites according to the cations (5A, 4A or 3A). The ZSM-5 structure is based on an assembly of MFI CBU's (Composite Building Units) mainly. This assembly gives rise to a two-dimensional structure composed of straight and sinusoidal channels of 5.1×5.5 Å and 5.3×5.6 Å respectively. The intersections of these channels have a diameter of approximately 6–8 Å (Losch 2016). The typical Si/Al ratio is 30 but it can be broadly modified, allowing structures with very high ratios (900). The pure silica form is commonly called silicalite. For an overview of CBU's and pseudo-structures, please see the reference (IZA 2019).

All the gases were provided by Linde Gas. Argon and helium were purchased in 6.0 quality (purity ≥ 99.9999%) and carbon dioxide, nitrogen and methane in 4.5 (purity ≥ 99.995%).

2.2 Methods

Table 2 shows the temperature and pressure ranges covered in this work by each experimental technique. These thermodynamic conditions correspond to the typical operating conditions of the different gas separation issues.

#### 2.2.1 Gas porosimetry with argon at 87 K

The samples were fully characterized in terms of textural properties using gas porosimetry technique with the aim to obtain the pore volume, the pore size distribution (PSD) and the BET surface. Argon adsorption–desorption isotherms at 87 K were performed using an Autosorb iQ (Quantachrome, US) with the Cryosync® temperature regulation system.

Table 1 Zeolite samples studied in this work

Zeolite	Structure	Molar Si/Al ratio	Cation	Windows (Å)	Cages (Å)	2D channels (Å)
13X	FAU	1–1.5	Na^+	7.4	13	–
5A	LTA	1	Na^+, Ca^{2+}	5	11.4	–
4A	LTA	1	Na^+	4	11.4	–
ZSM-5(58)	MFI	58	NH_4^+	–	–	5.2
ZSM-5(295)	MFI	295	NH_4^+	–	–	5.2

Table 2 Performed measurements according to each experimental technique

	High resolution low pressure manometry		High pressure gravimetry		Calorimetry	
	T (K)	P (bar)	T (K)	P (bar)	T (K)	P (bar)
13X						
CO_2	273–363	0–1	273–363	1–20	313–383	0–9
N_2	–	–	293–363	0–10	313	
CH_4	–	–	273–363	1–80	313	
5A						
CO_2	253–353	0–1	253–353	1–20	313–383	0–9
N_2	–	–	293–363	0–10	313	
CH_4	–	–	253–363	1–80	313	
4A, ZSM-5(58), ZSM-5(295)						
CO_2	273–363	0–1	273–363	1–20	–	
N_2	–	–	293–363	0–10	–	
CH_4	–	–	273–363	1–80	–	
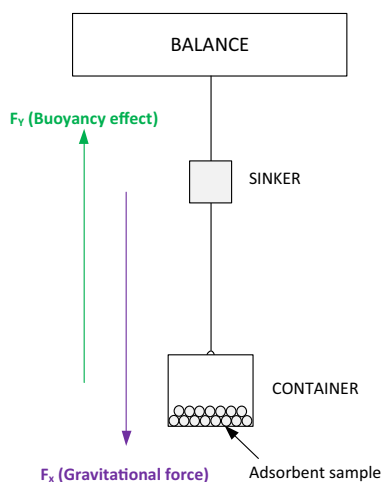
Fig. 1 Forces balance of Rubotherm system

In order to eliminate any trace of gas prior to any experiment, all the samples were degassed during 12 h at 573 K under secondary vacuum (heating ramp of 10 K min⁻¹). For further details on these pretreatment conditions, please see the references (Lowell et al. 2010; Wang and LeVan 2009).

2.2.2 High pressure gravimetry

High pressure isotherms were performed by means of a Magnetic Suspension Balance (Rubotherm, Germany). The system is fully automated and can operate from primary vacuum up to 150 bar within a temperature range of − 20 to 400 °C. A homemade electrical heating system allows to pretreat the sample at high temperatures.

Figure 1 shows the scheme of the forces balance of the Rubotherm magnetic suspension system. It is composed of

an electromagnet linked to a permanent magnet that holds a suspension consisting of a container where the sample is introduced and a sinker (steel volume of known density) that allows measuring the density of the bulk phase directly. The magnetic suspension switches between three positions: ZP (zero point), MP1 (measuring point 1) and MP2 (measuring point 2). In ZP position, the suspension without the container and the sinker is raised. In MP1 the container is also raised and in the MP2 position the weight corresponds to the whole magnetic suspension including the sinker.

The buoyancy effect and the gravitational force can be calculated as follows:

$$(Buoyancy) F_y = \left[\left(V_{container} + V_{adsorbed} + V_{sample} + V_{sinker} \right) \rho_{bulk,g} \right] g \quad (1)$$

$$(Gravitational force) F_x = \left(m_{container} + m_{adsorbed} + m_{sample} + m_{sinker} \right) g \quad (2)$$

where V and m denote respectively the volume and the mass of all the components of the magnetic suspension and the adsorbed phase. The bulk density of the gas is denoted $\rho_{bulk,g}$ and g refers to the gravitational constant. The subtraction of buoyancy from gravitational force allows the calculation of the resulting force F_r:

$$F_r = \left(m_{container} + m_{adsorbed} + m_{sample} + m_{sinker} \right) g - \left[\left(V_{container} + V_{adsorbed} + V_{sample} + V_{sinker} \right) \rho_{bulk,g} \right] g \quad (3)$$

Three steps have to be performed to measure the pure gas adsorption equilibria. The principle of the different steps and the obtained data is presented in Table 3.

In this publication we show the way to calculate the uncertainties according to the GUM (Guide to the expression of Uncertainty in Measurement) method (BIPM 2008)

Table 3 Different steps for pure gas equilibrium measurement

Step	Principle	Obtained data
Blank	Several isothermal pressure steps without sample	Mass and volume of the container
Buoyancy	Several isothermal pressure steps with the sample using a non-adsorbed gas (ex: helium)	Mass and volume of the sample
Adsorption equilibrium	Several isothermal pressure steps with the sample using an adsorbed gas	Adsorbed excess mass of the gas

for the Magnetic Suspension Balance of Rubotherm (Germany). This method lists all the properties influencing the measurement and combines them using the mathematical model of the measurement. The uncertainty is then evaluated according to the law of propagation of uncertainties and a multiplier coefficient is applied in order to weight the uncertainty with a level of confidence determined by the law of probability.

From the force balance of the Rubotherm system presented in Fig. 1 in MP1 position, the absolute adsorbed amount can be calculated as follows:

$$m_{adsorbed} = (m_{r,MP1} - m_{container} - m_{sample}) + \rho_{g,bulk}(V_{container} + V_{sample} + V_{adsorbed}) \quad (4)$$

As the properties of the adsorbed phase cannot be obtained experimentally, the excess adsorbed amount is calculated as:

$$m^{excess} = m_{adsorbed} - \rho_{g,bulk}V_{adsorbed} = (m_{r,MP1} - m_{container} - m_{sample}) + \rho_{g,bulk}(V_{container} + V_{sample}) \quad (5)$$

Due to the buoyancy effect, the sinker weight will differ with the pressure and temperature of the surrounding fluid. This phenomenon is used to calculate the density of the fluid:

$$\rho_{bulk,g} = \frac{(m_{sinker,vacuum} - m_{sinker,i})}{V_{sinker}} \quad (6)$$

Table 4 Standard uncertainty of each magnitude

Variable	Uncertainty
m_{MP1}, m_{MP2}	Stability of the balance fixed at 50 µg
$m_{container}$	Repeatability of blank measurements
m_{sample}	Repeatability of buoyancy measurements
$V_{container}$	Repeatability of blank measurements
V_{sample}	Repeatability of buoyancy measurements
m_{sinker}	Provided by the supplier
v_{sinker}	Provided by the supplier

The mass of the sinker at each pressure and temperature conditions can be calculated from MP2 and MP1 positions as follows:

$$m_{sinker,i} = MP2_i - MP1_i \quad (7)$$

Equations 5, 6 and 7 constitute the measurement model and contain the main properties that can have an impact on the measurement. The standard uncertainty of each property can be evaluated as indicated in Table 4.

According to the propagation of uncertainties, the uncertainty of m^{excess}, $\rho_{g,bulk}$ and $m_{sinker,i}$ can be evaluated as follows:

$$\Delta m_{sinker,i} = K\sqrt{\left|\frac{\delta m_{sinker,i}}{\delta m_{MP2_i}}\right|^2 (\Delta m_{MP2_i})^2 + \left|\frac{\delta m_{sinker,i}}{\delta m_{MP1_i}}\right|^2 (\Delta m_{MP1_i})^2} \quad (8)$$

$$\Delta\rho_{g,bulk} = K\sqrt{\left|\frac{\delta\rho_{g,bulk}}{\delta m_{sinker,vacuum}}\right|^2 (\Delta m_{sinker,vacuum})^2 + \left|\frac{\delta\rho_{g,bulk}}{\delta m_{sinker,i}}\right|^2 (\Delta m_{sinker,i})^2 + \left|\frac{\delta\rho_{g,bulk}}{\delta V_{sinker}}\right|^2 (\Delta V_{sinker})^2} \quad (9)$$

$$\Delta m^{excess} = K\sqrt{\begin{array}{l}\left|\frac{\delta m^{excess}}{\delta m_{r,MP1}}\right|^2 (\Delta m_{r,MP1})^2 + \left|\frac{\delta m^{excess}}{\delta m_{container}}\right|^2 (\Delta m_{container})^2 + \left|\frac{\delta m^{excess}}{\delta m_{sample}}\right|^2 (\Delta m_{sample})^2 \\ + \left|\frac{\delta m^{excess}}{\delta\rho_{g,bulk}}\right|^2 (\Delta\rho_{g,bulk})^2 + \left|\frac{\delta m^{excess}}{\delta V_{container}}\right|^2 (\Delta V_{container})^2 + \left|\frac{\delta m^{excess}}{\delta V_{sample}}\right|^2 (\Delta V_{sample})^2\end{array}} \quad (10)$$

In all these equations K is a weighting factor that allows to give the uncertainty with a confidence level of 95%.

2.2.3 High resolution low pressure manometry

Carbon dioxide high resolution low pressures isotherms (up to 1 bar) at several temperatures were carried out with an Autosorb iQ (Quantachrome, US). Temperature regulation was implemented with a double jacket Dewar and a thermostatic bath.

Concerning the manometric system, the Autosorb iQ commercial apparatus uses an algorithm called maxidose® to reach the targeted points of relative pressures. As there is not access to this algorithm the uncertainty of the measurements could not be evaluated.

2.2.4 Calorimetry

Calorimetric data were obtained with a Tian Calvet Setaram C80 differential heat flow calorimeter coupled with a homemade manometric system operating isothermally. For further details of the system, see the reference (Mouahid et al. 2012). The calculation of the differential heat of adsorption and the measurement uncertainty is detailed in the previous reference. More precisely, the estimated measurement uncertainty is approximately 5%.

3 Modeling of pure gas adsorption

Due to their simplicity, their ability to fit the experimental data at low and high pressures and their straightforward implementation in numerical simulations of industrial adsorption processes, kinetical and semi-empirical equilibrium models such as Langmuir, bi-Langmuir, Toth and Sips (Do 1998; Yang 1999) are widely used. In this section the theoretical basis of each model are briefly reminded.

3.1 Langmuir and bi-Langmuir models

In its usual form, the Langmuir model (Langmuir 1918) is used for the description of the adsorption of monolayers on homogeneous surfaces. It is based on four main hypotheses: the adsorption of a molecule is localized; each adsorption site can accommodate only one molecule; the energy of adsorption is constant over all the adsorption sites and there is no interaction between neighboring adsorbents. The Langmuir model adopts the following form:

$$q_e = \frac{q_m b P}{1 + bP} \tag{11}$$

where q_e is the amount adsorbed; q_m is the saturation capacity (monolayer coverage); b is the affinity constant and P is the pressure of the gas. The Langmuir model can also be used to describe the adsorption on heterogeneous surfaces. It is assumed that the surface contains several regions from an energetic point of view and each region follows the usual Langmuir assumptions. If two regions are considered, the model is called bi-Langmuir and consists of two Langmuir terms, each one corresponding to a region:

$$q_e = \frac{q_{m,1} b_1 P}{1 + b_1 P} + \frac{q_{m,2} b_2 P}{1 + b_2 P} \tag{12}$$

where $q_{m,1}$ and $q_{m,2}$ are the saturation capacity of the first and the second region respectively and b_1 and b_2 are the affinity constants of each region.

The affinity constant and the saturation capacity vary with temperature as follows:

$$b = b_0 e^{\left(\frac{Q}{RT}\right)} \tag{13}$$

$$q_m = q_{0exp}\left(-\gamma\left(T - T_0\right)\right) \tag{14}$$

where b_0 is the affinity constant at some reference temperature; Q is a representative parameter of the heat of adsorption; R is the ideal gas constant and T the temperature; q_0 is the saturation capacity at a reference temperature, T_0 is the reference temperature and γ the thermal expansion of the adsorbed phase.

By applying the van't Hoff equation to the Langmuir type model, the prediction of the isosteric heat of adsorption is obtained as:

$$\frac{\Delta H}{RT^2} = -\left(\frac{d ln P}{dT}\right)_{qe} \rightarrow (-\Delta H) = \frac{\sum_{j=1}^{N} q_{m,j} \frac{b_j Q_j}{(1+b_j P)^2}}{\sum_{j=1}^{N} q_{m,j} \frac{b_j}{(1+b_j P)^2}} \tag{15}$$

where ΔH represents the isosteric heat of adsorption and N is the number of Langmuir terms considered.

3.2 Toth's model

This semi-empirical model (Toth 1971) is based on the Langmuir equation. A parameter t (that is usually less than unity) has been added to the Langmuir's model by Toth in order to take into account the heterogeneity of the system (adsorbent–adsorbate). For t = 1 the system is considered as homogeneous and the expression reduces to the Langmuir equation.

$$q_e = \frac{q_m bP}{1 + \left[(bP)^t\right]^{1/t}} \tag{16}$$

The variation of t with temperature is empirical and given by:

$$t = t_0 + \alpha\left(1 - \frac{T_0}{T}\right) \tag{17}$$

where t_0 is the heterogeneity parameter at a reference temperature and α is a constant.

The isosteric heat of adsorption corresponding to this model can be directly obtained from the Van't Hoff equation and is as follows:

$$(-\Delta H) = Q - \frac{1}{t}(\alpha RT_0)\left\{\ln(bP) - \left[1 + (bP)^t\right]ln\left[\frac{bP}{\left(1 + (bP)^t\right)^{\frac{1}{t}}}\right]\right\} \tag{18}$$

3.3 Sips or Langmuir–Freundlich model

The Sips equation of adsorption (Sips 1948) was proposed as an alternative to Freundlich equation so that adsorption tends to a finite limit at high pressure. This equation takes the following form:

$$q_e = \frac{q_m (bP)^{1/n}}{1 + (bP)^{1/n}} \tag{19}$$

In the same way as the Toth model, this equation is similar to that of Langmuir, with the addition of the parameter n that takes into account the system's heterogeneity. When this parameter is 1 (ideal surface), the Langmuir equation is recovered. The parameter n evolves with temperature according to an empirical form:

$$\frac{1}{n} = \frac{1}{n_0} + \alpha\left(1 - \frac{T_0}{T}\right) \tag{20}$$

where n_0 is the heterogeneity parameter at a reference temperature and α is a constant.

The isosteric heat can be calculated from the following expression:

$$(-\Delta H) = Q - (\alpha RT_0) n ln(bP) \tag{21}$$

3.4 Isosteric heat calculation from differential heat of adsorption measurements

The isosteric heat of adsorption is the difference between the enthalpy of the equilibrium gas phase and the enthalpy of the adsorbed phase. It can be calculated from the

Clausius–Clapeyron equation assuming that the gas phase behaves as an ideal phase and that the volume of the adsorbed phase is negligible in comparison with the volume of the gas phase (Zukal et al. 2010):

$$(-\Delta H) = RT^2\left(\frac{dlnP}{dT}\right)_{qe} = (-\Delta_{ads}H) + RT \tag{22}$$

where $(-\Delta_{ads}H)$ is the differential enthalpy of adsorption.

3.5 Excess and absolute adsorption

Using gravimetric and manometric techniques, without any information about the properties of the adsorbed phase, it is not possible to get access to the absolute amount adsorbed in the material. To overcome this problem, the concept of excess amount adsorbed was introduced by Gibbs in order to describe the amount of fluid close to the adsorbent surface at a concentration above that of the bulk phase (Gibbs 1877). The excess adsorption is related to the absolute adsorption by the following expression:

$$m^{excess} = m_{adsorbed} - \rho_{g,bulk} V_{adsorbed} \tag{23}$$

At high pressures, when the pores are saturated and the density of the bulk phase becomes high, it is typical to observe a decrease in the excess adsorption isotherm. That is the case for methane in this work. Thus, excess adsorption rather than absolute adsorption has to be modeled. In this way, Eq. 23 can be transformed as follows:

$$m^{excess} = m_{adsorbed} - \rho_{g,bulk}\frac{m_{adsorbed}}{\rho_{adsorbed}}$$
$$\rightarrow m^{excess} = m_{adsorbed}(1 - \frac{\rho_{g,bulk}}{\rho_{adsorbed}}) \tag{24}$$

where $\rho_{adsorbed}$ is the density of the adsorbed phase which can be approximated from the saturation capacity and the pore volume calculated from argon isotherms at 87 K:
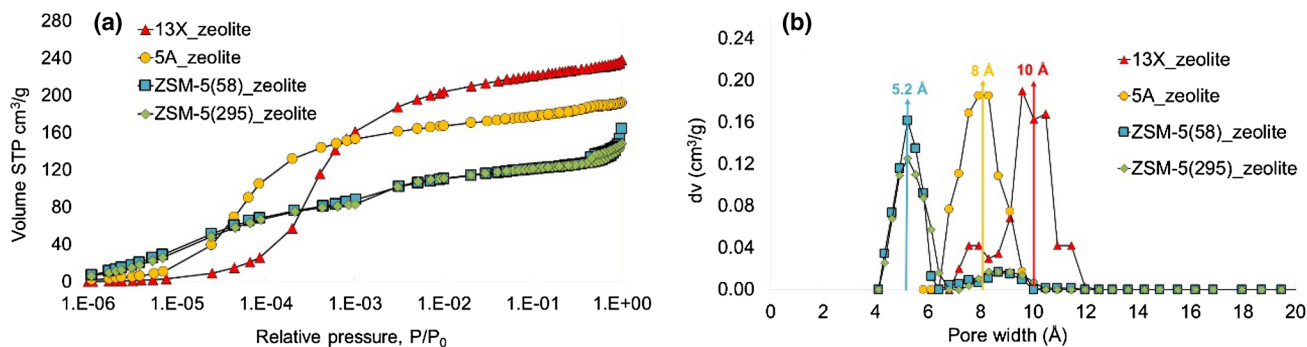
$$m^{excess} = m_{adsorbed}\left(1 - \frac{\rho_{g,bulk}}{\frac{q_m M_m}{V_p}}\right) \tag{25}$$

M_m is the molar mass of the adsorbate and V_p is the pore volume.

4 Results and discussion

4.1 Gas porosimetry with argon at 87 K

Figure 2a shows the argon adsorption–desorption isotherms at 87 K on the different zeolites, except the 4A, within the

Fig. 2 **a** Argon adsorption–desorption isotherms on different zeolites (semi-logarithmic scale) and **b** pore size distribution of different zeolites obtained with NLDFT models (Quantachrome software)

whole range of relative pressures. Indeed, significant diffusional limitations and molecular crowding phenomena are encountered for pore sizes lower than 4.5 Å for argon adsorption at 87 K (Thommes et al. 2015) which prevents from analyzing the 4A zeolite with this gas at these conditions.

Although 13X and 5A zeolites are composed of windows and cages of different sizes, a two-step pore filling mechanism is not observed. The low-pressure part of the adsorption isotherm has a slight slope that can be interpreted as the adsorption of argon molecules around the windows of the zeolite. After that, a steeper slope that represents the filling of the structure is observed. Higher pore filling relative pressures indicate a greater pore size in the case of 13X zeolite. In the same way, the higher adsorption capacity of 13X zeolite suggests a higher pore volume. The argon isotherm on ZSM-5 zeolites shows a continuous increase of the adsorbed amount, typical of a structure consisting of channels. The overlap of the isotherms of argon on the ZSM-5 zeolites with different Si/Al ratio confirms that argon is not sensitive to differences in surface chemical properties (Thommes et al. 2012). A change in the slope is observed at a relative pressure of about 1E-3. This phenomenon is not fully understood today and has been attributed either to a zeolite phase transition (orthorhombic to monoclinic) or to an adsorbate phase transition (from liquid-like to solid-like state) (Thommes et al. 2012; Llewellyn et al. 1993).

The Pore Size Distribution of each sample is presented in Fig. 2b) and was obtained by applying the NLDFT models available in the Autosorb software for argon adsorption at 87 K on zeolites. A cylindrical/spherical pore model was applied to 13X and 5A zeolites and a cylindrical pore model was applied to ZSM-5. The obtained pore size for ZSM-5 zeolites coincides with the theoretical pore size at 5.2 Å. In addition, the additional pore size that appears at 9 Å is not a real pore and is related to the phase transition phenomena already mentioned. Because of the continuous filling of the windows and cages in the case of 5A and 13X zeolites, the obtained PSD is centered on an intermediate size between the ones of the windows and cages. Thus, the calculated pore sizes are approximately 10 Å and 8 Å for 13X and 5A zeolites respectively.

The pore volume calculated by NLDFT models and the BET surface obtained according to the procedure for microporous adsorbents defined by Rouquerol et al. (2007) are reported in Table 5.

4.2 Experimental adsorption isotherms—high resolution low pressure manometry and high pressure gravimetry

As an example of the results obtained in this work, Fig. 3 shows the adsorption isotherms of the different gases on 5A zeolite at several temperatures. The CO_2 isotherms are composed of the data obtained by high resolution low pressure manometry (up to 1 bar) and experimental points obtained by high pressure gravimetry (up to 20 bar). The coupling of both methods allows to observe for the first time the successive CO_2 adsorption mechanisms over seven decades of pressures with accuracy. As seen in the graphs, all the isotherms are typical of microporous adsorbents and nitrogen and methane fill the pores at higher pressures than CO_2. The gas/zeolite interactions, greater for CO_2 than for N_2 and CH_4 (presence of specific sites on the surface of the zeolite and greater quadrupolar moment of CO_2 molecules), shift the pore filling region to

Table 5 BET surface and micropore volumes of different samples

Zeolite sample	13X	5A	4A	ZSM-5(58)	ZSM-5(295)
BET surface (m²/g)	799	641	–	434	435
Pore volume (NLDFT) (cm³/g)	0.37	0.35	–	0.22	0.21
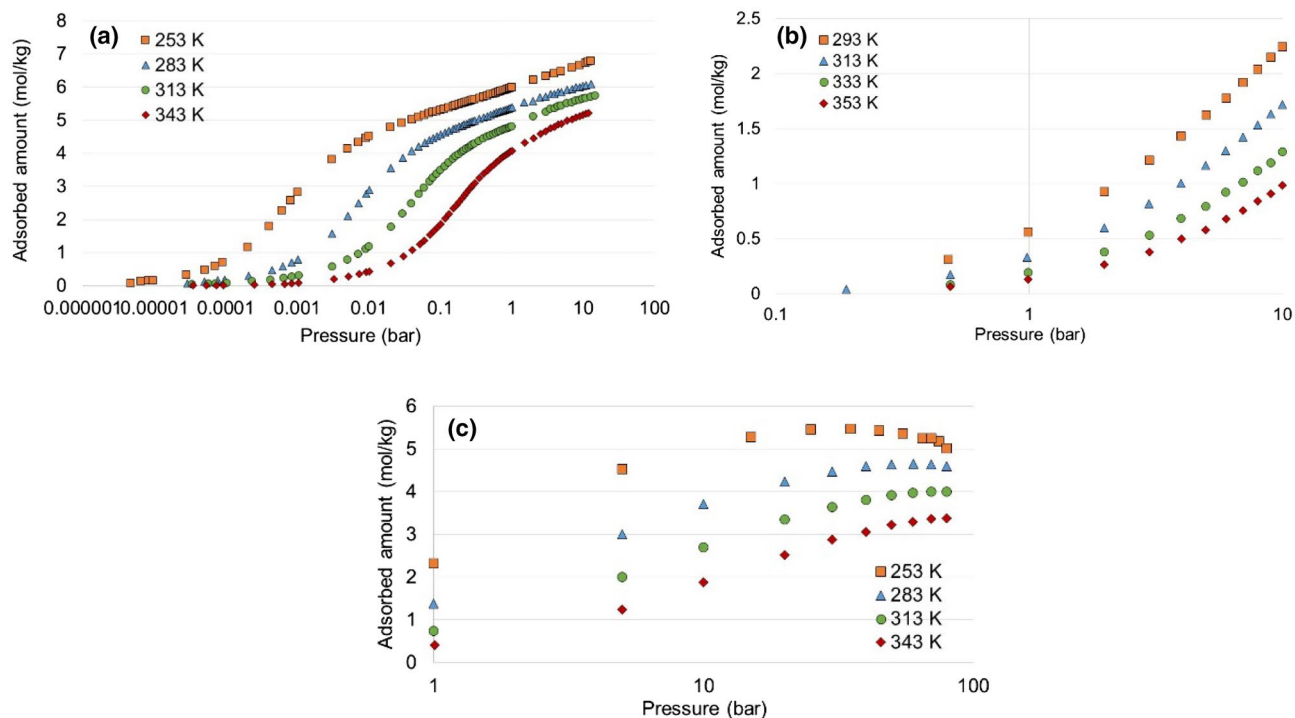
Fig. 3 Adsorption–desorption isotherms on 5A zeolite (semilogarithmic scale) at different temperatures. **a** CO_2, **b** N_2 and **c** CH_4

Table 6 Example of the uncertainty calculation for the adsorption equilibrium measurements using gravimetric method. Adsorption of different gases on 5A zeolite at 313 K

	CO_2		N_2		CH_4	
	2 bar	15 bar	3 bar	10 bar	5 bar	70 bar
$\left\|\dfrac{\delta m^{excess}}{\delta m_{r,MP1}}\right\|^2 \times \left(\Delta m_{r,MP1}\right)^2$	1.8E−9 (3.2%)	1.2E−10 (0.2%)	2.7E−11 (0%)	3.2E−11 (0.1%)	1.3E−10 (0.2%)	3.6E−10 (0.3%)
$\left\|\dfrac{\delta m^{excess}}{\delta m_{container}}\right\|^{2*} \left(\Delta m_{container}\right)^2$	3.4E−8 (59.7%)	3.4E−8 (41.7%)	3.4E−8 (62%)	3.4E−8 (60.6%)	3.4E−8 (61.7%)	3.4E−8 (24.4%)
$\left\|\dfrac{\delta m^{excess}}{\delta m_{sample}}\right\|^2 \times \left(\Delta m_{sample}\right)^2$	1.6E−8 (28.1%)	1.6E−8 (19.6%)	1.6E−8 (29.2%)	1.6E−8 (28.4%)	1.6E−8 (29%)	1.6E−8 (11.5%)
$\left\|\dfrac{\delta m^{excess}}{\delta \rho_{g,bulk}}\right\|^2 \times \left(\Delta \rho_{g,bulk}\right)^2$	4.6E−9 (8%)	4.6E−9 (5.6%)	4.4E−9 (8%)	4.5E−9 (8%)	4.6E−9 (8.3%)	6.2E−9 (4.4%)
$\left\|\dfrac{\delta m^{excess}}{\delta V_{container}}\right\|^2 \times \left(\Delta V_{container}\right)^2$	1.2E−10 (0.2%)	7.8E−9 (9.6%)	1.1E−10 (0.2%)	4.4E−10 (0.9%)	1.1E−10 (0.2%)	2.4E−8 (17.2%)
$\left\|\dfrac{\delta m^{excess}}{\delta V_{sample}}\right\|^2 \times \left(\Delta V_{sample}\right)^2$	4.3E−10 (0.8%)	1.9E−8 (23.3%)	2.7E−10 (0.6%)	1.1E−9 (2%)	2.7E−10 (0.6%)	5.9E−8 (42.3%)
	5.8E−8	8.2E−8	5.5E−8	5.7E−8	5.5E−8	1.4E−7
Total uncertainty (g) (95%)	4.80E−4	5.8E−4	4.7E−4	4.8E−4	4.7E−4	7.5E−4
Mass adsorbed (g)	8.20E−2	9.2E−2	8.9E−3	1.4E−2	1.2E−2	2.4E−2
Relative uncertainty (%)	0.59	0.62	5.31	3.45	3.9	3.15

lower pressures for this adsorbate. The same trend is observed for all the other zeolites studied in this work. The isotherms concerning the other gases and zeolites are presented in the supplementary information provided with this publication.

It should be pointed out that the shape of CO_2 isotherms at several temperatures are similar for all the adsorbents except for the 4A zeolite, indicating the same adsorption mechanism at each temperature. In the case of CO_2 adsorption on the 4A

zeolite, an inflection point at about 0.01 bar is only observed at 273 K, suggesting that the adsorption mechanism at low temperature (273 K) is not the same that at high temperature (363 K). This fact could be related to the mobility of cations already observed for this adsorbent (Akten et al. 2003). However, further investigations are needed to clarify this point.

In Table 6 an example of the uncertainty calculation using the gravimetric method at 313 K is shown on the 5A zeolite. From Eq. 10, one can calculate the sum of the terms inside the square root and evaluate the contribution of each measured property to the final value of the uncertainty. Two examples, at low and at high pressure, are given for each gas in order to analyze how each term evolves with pressure. As a general comment, the relative uncertainty values are very low and the measurements are accurate. As the total uncertainty values are similar for all the gases at a confidence level of 95%, the relative uncertainty depends predominantly on the amount adsorbed. More specifically, at low pressures, when the buoyancy effect is negligible, the main contributions to the uncertainty are the masses of the container and the sample determined from the blank and buoyancy measurements. On the other hand, at higher pressures, when buoyancy effect is significant, the uncertainties corresponding to the volumes of the container and the sample become important. It should be noted that the difference between manometry and gravimetric data is about 2% showing a very good agreement between the two techniques. It can be deduced that the uncertainty of the manometric measurements, which can be high and overestimated when evaluated with the propagation of errors (Wiersum 2012) is also low.

4.3 Experimental calorimetric results

More detailed information about the adsorption mechanisms may be obtained from calorimetry experiments. Figure 4 shows the experimental results of the differential heat of adsorption of the different gases on the 5A and 13X zeolites as a function of pressure. The experiments concerning CO_2 were performed at three temperatures (between 313

and 383 K) in order to analyze the influence of this variable on the differential heat of adsorption. To our knowledge, no experimental heats of adsorption have ever been published for CO_2, N_2 and CH_4 on 5A zeolite. The results obtained on the 13X zeolite could be compared with other literature sources (Dunne et al. 1996b; Bourrelly et al. 2005; Zimmermann and Keller 2003) at the lowest temperature. A very good agreement is observed between these data.

All the heats of adsorption decrease at low pressures. This variation at low filling is attributed to the surface heterogeneity caused by the presence of specific adsorption sites. Once these specific sites are occupied and saturated, the adsorbate fills the void space of the pores and the adsorbate–adsorbate–adsorbent interactions predominate, leading to a constant heat of adsorption upon increasing pressure. Indeed, the extra-framework cations present in the zeolites have been identified as the specifics sites of adsorption in several microscopic studies (Zukal et al. 2011; Montanari and Busca 2008; Newsome et al. 2014; Maurin et al. 2005). The interaction between molecules and cation sites are electrostatic and are mainly controlled by the quadrupole moment of the adsorbates. As the quadrupole moment of CO_2 is much greater than those of nitrogen and methane, the interaction with the electric field induced by the presence of the cations and the value of the differential heat of adsorption are higher for CO_2 (Bonenfant et al. 2008; Tagliabue et al. 2009). In the case of methane, which does not have a quadrupole moment, the adsorption is mainly controlled by its polarizability. Small differences were observed between the differential heats of adsorption at 313 K and at 383 K in the pressure range of the CO_2-cations interactions.

A comparison of the evolution of the differential heat of adsorption of each adsorbate on different zeolites is depicted in Fig. 5. As no calorimetric measurements were performed for ZSM-5 zeolites in this work, data at temperatures around 313 K have been taken from literature (Dunne et al., 1996a, b). These data correspond to two similar zeolites to those
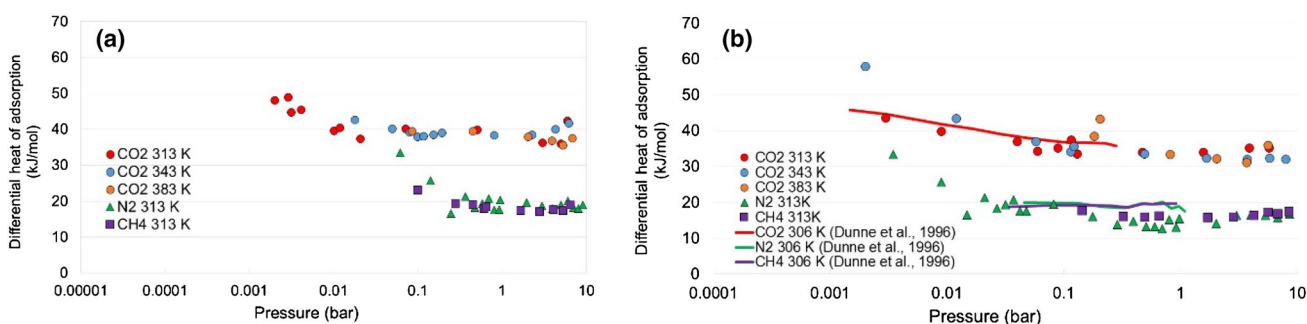
Fig. 4 Experimental heats of adsorption results of CO_2 at different temperatures (in semilogarithmic scale) and N_2 and CH_4 at 313 K. **a** 5A zeolite and **b** 13X zeolite
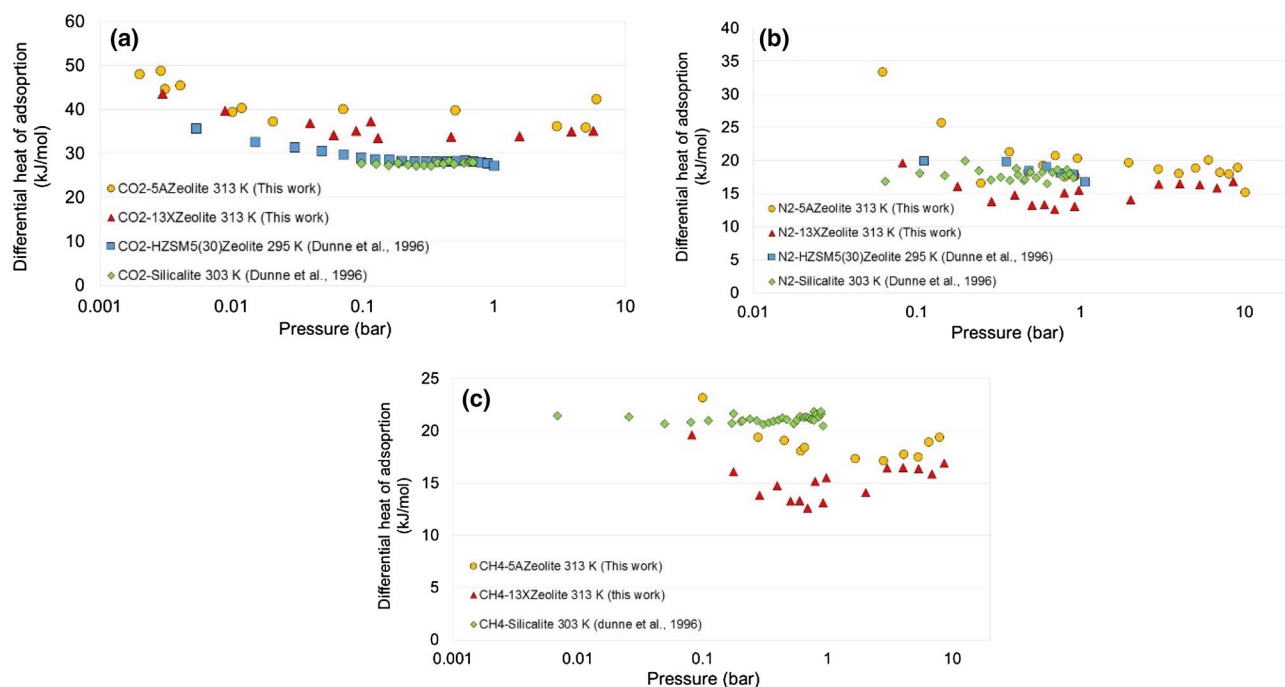
Fig. 5 Differential heat of adsorption around 313 K on 5A, 13X, HZSM5 (30) and silicalite zeolites (semilogarithmic scale). **a** CO_2, **b** N_2 and **c** CH_4
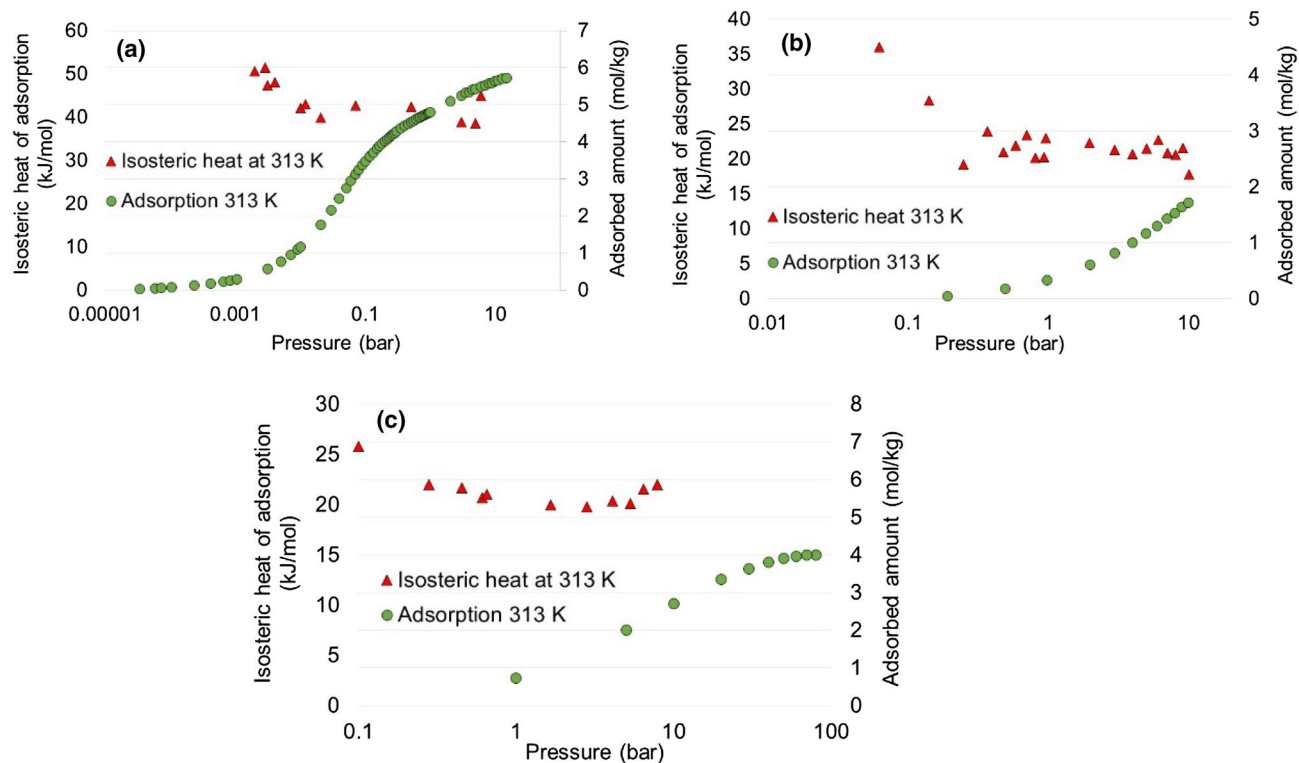
Fig. 6 Coupling of adsorption equilibria with the isosteric heat of adsorption obtained from calorimetric results on 5A zeolite. **a** CO_2, **b** N_2 and **c** CH_4

considered in this work: HZSM-5 with a Si/Al ratio of 30 and silicalite. From Fig. 5a), it may be inferred that the heat of adsorption of CO_2 is largely influenced by the Si/Al ratio of the adsorbent suggesting that the adsorption is mainly controlled by the adsorbate–cation interactions. On the other hand, within the pressure range considered in this work, nitrogen and methane differential heats of adsorption on the different zeolites shows a constant trend, suggesting that the adsorption is mainly controlled by the adsorbate–adsorbate–adsorbent interactions during pore filling mechanism.

4.4 Understanding the mechanisms of adsorption–coupling experimental adsorption isotherms with calorimetric data

The coupling of calorimetric data with adsorption isotherms allows to better understand which pressure regions are controlled by adsorbate–cation interactions (adsorption on specific sites) or by adsorbate–adsorbate–surface interactions (pore filling). In this way, Fig. 6 shows the coupling of the isosteric heat and the adsorption isotherms at 313 K. The isosteric heat was calculated according to Eq. 22. It is plotted in these figures because it is an important property for the assessment of equilibrium models, as shown in Sect. 4.5 of this publication. One can conclude that, at this temperature, CO_2 adsorption is governed by the interactions with cations up to approximately 0.1 bar and then, pore filling mechanism is observed until 20 bar. On the other hand, only pore filling mechanism should be considered for nitrogen and methane within the range of operating conditions considered in this work.

Finally, the comparison of the adsorption isotherms of the three gases on all the zeolites at 313 K (Fig. 7), confirms what have been discussed above. Two regions are clearly identified in the CO_2 adsorption isotherms. In the low-pressure region—up to approximately 0.1 bar—the amount adsorbed is directly related to the Si/Al ratio of the zeolites and therefore the concentration of cations. For the higher pressures, the adsorbed amount depends on the pore volume (see Table 5). On the other hand, at these conditions, the adsorbed amount of nitrogen and methane varies only with the pore volume.

4.5 Assessment of classical thermodynamic models

The fitting of the Toth, Sips and bi-Langmuir equations was performed by minimizing the square of residuals (SOR) at each temperature:
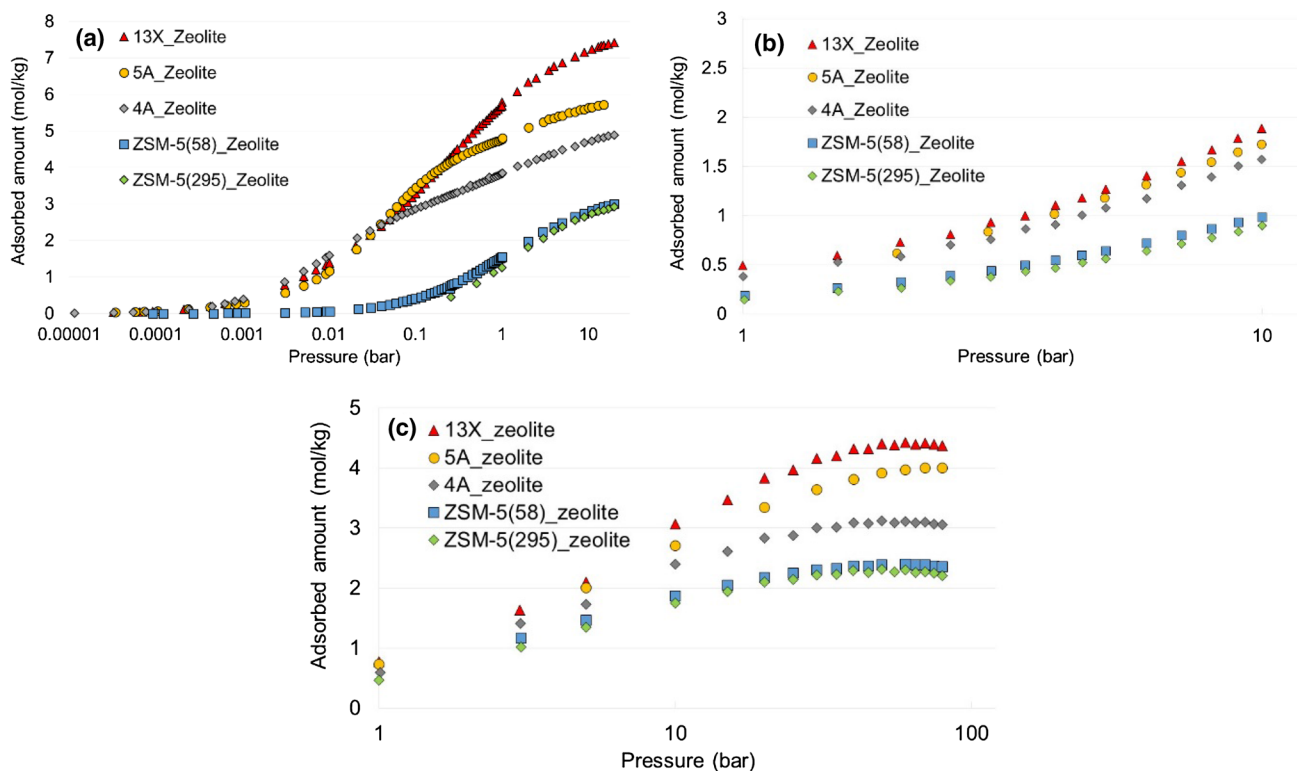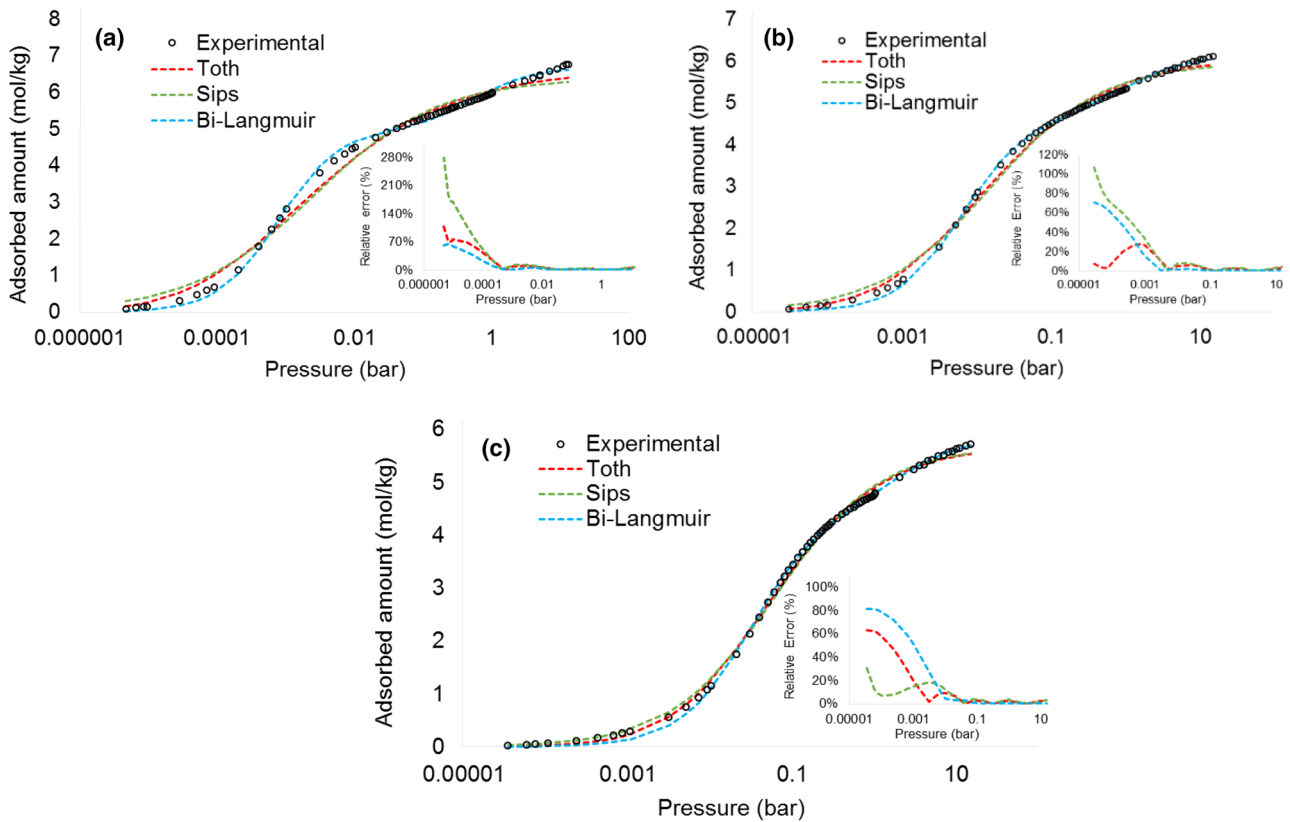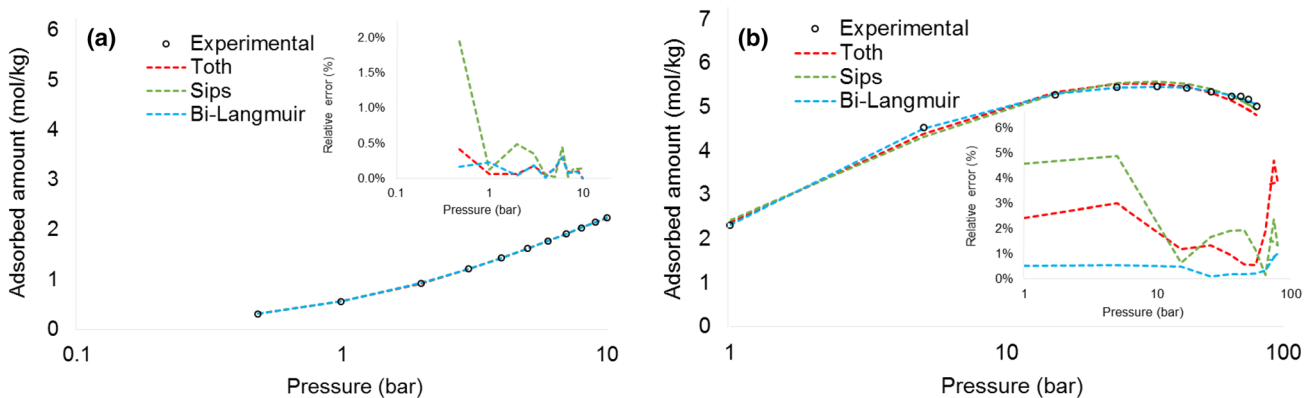

Fig. 7 Adsorption–desorption isotherms on different zeolites at 313 K. **a** CO_2, **b** N_2 and **c** CH_4

Fig. 8 Toth, Sips and bi-Langmuir modeling comparison of the CO_2 adsorption on 5A zeolite at several temperatures. **a** 253 K, **b** 283 K, and **c** 343 K
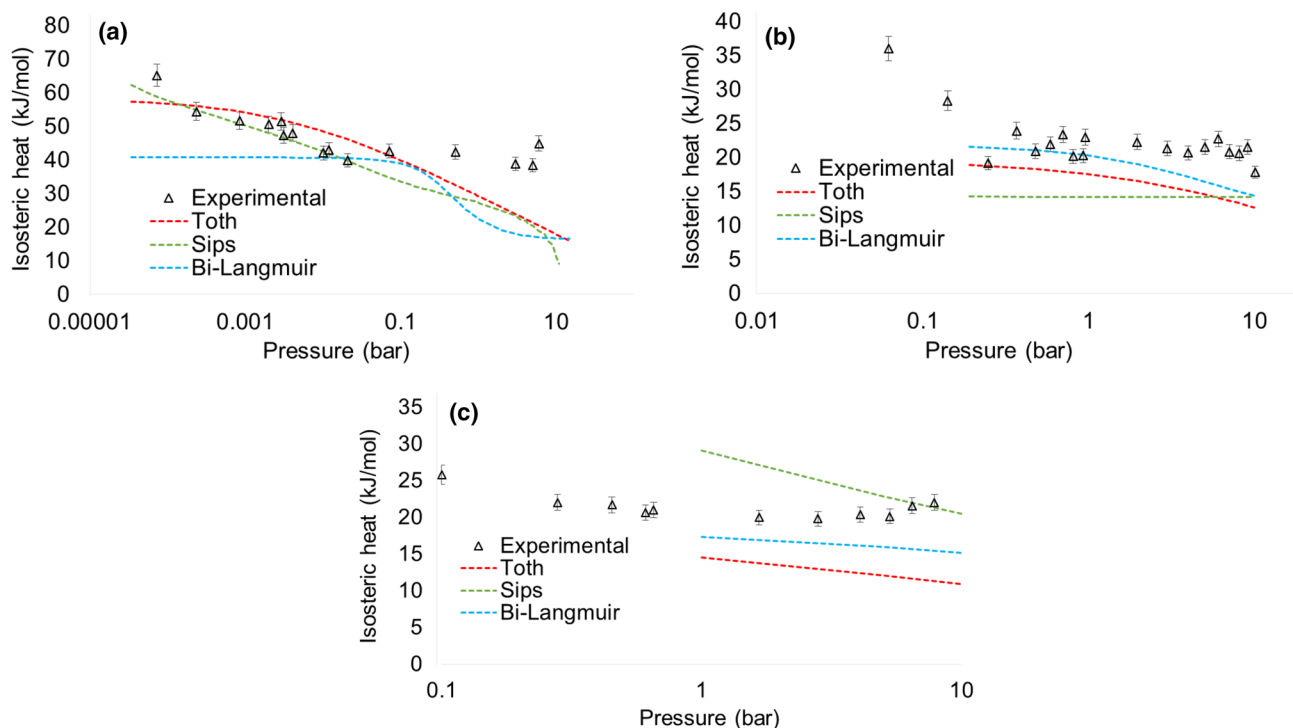

Fig. 9 Toth, Sips and bi-Langmuir modeling comparison of the N_2 and CH_4 adsorption on 5A zeolite. **a** N_2 adsorption at 293 K and **b** CH_4 adsorption at 253 K

$$SOR = \sum_{i=1}^{n} \left(q_{eq,th} - q_{eq,exp} \right)^2 \qquad (26)$$

where n is the number of experimental points (P, $q_{eq,exp}$) per isotherm.

The comparison of the fitting of the different models to experimental data of CO_2 adsorption on 5A zeolite at 253 K, 283 K and 313 K is depicted in Fig. 8. From this comparison it can be inferred that none of the models is able to fit the experimental data (especially at low pressures) over the whole range of operating conditions. However, bi-Langmuir

Fig. 10 Toth, Sips and bi-Langmuir isosteric heat predictions comparison on 5A zeolite. **a** CO_2, **b** N_2 and **c** CH_4

Table 7 Toth, Sips and bi-Langmuir parameters and objective function of the modeling of CO_2, N_2 and CH_4 adsorption on 5A zeolite at several temperatures

T(K)	CO_2				N_2				CH_4			
	253	283	313	343	293	313	333	353	253	283	313	343
Toth												
q_m (mol/kg)	6.64	6.12	5.72	5.35	4.90	3.68	3.54	3.30	6.97	7.28	6.88	6.31
b (bar^{-1})	11,797.91	522.21	52.87	8.00	0.17	0.11	0.06	0.04	0.88	0.62	0.22	0.09
t	0.36	0.47	0.59	0.74	0.68	0.88	0.93	0.95	0.69	0.50	0.54	0.60
SOR (mol/kg)^2	2.2	0.8	2.3	0.3	5.10^{-5}	9.10^{-4}	1.10^{-3}	5.10^{-5}	5.10^{-2}	1.10^{-2}	6.10^{-3}	3.10^{-3}
Sips												
q_m (mol/kg)	6.39	5.97	5.68	5.44	4.11	3.75	3.37	3.10	7.19	7.06	6.41	5.82
b (bar^{-1})	383.62	66.54	16.34	4.32	0.12	0.09	0.06	0.05	0.38	0.12	0.06	0.04
n	2.08	1.73	1.48	1.31	1.14	1.07	1.01	1.00	1.46	1.59	1.42	1.29
SOR (mol/kg)^2	3.6	1.4	0.6	0.2	2.10^{-4}	5.10^{-3}	1.10^{-3}	6.10^{-4}	1.10^{-1}	3.10^{-2}	2.10^{-2}	5.10^{-3}
Bi-Langmuir												
$q_{m,1}$ mol/kg	4.97	4.66	4.44	4.22	3.25	2.50	1.59	1.28	5.89	4.66	4.07	3.60
b_1 (bar^{-1})	1304.17	161.33	32.25	7.76	0.09	0.08	0.07	0.06	0.65	0.38	0.19	0.10
$q_{m,2}$ (mol/kg)	1.71	1.48	1.44	1.34	0.81	0.90	1.76	1.97	3.07	5.47	5.14	4.45
b_2 (bar^{-1})	1.84	1.03	0.50	0.29	0.57	0.19	0.05	0.03	$2.6 \, 10^{-3}$	$2.5 \, 10^{-3}$	$2.4 \, 10^{-3}$	$2.4 \, 10^{-3}$
SOR (mol/kg)^2	0.6	0.2	0.2	0.1	6.10^{-5}	8.10^{-4}	1.10^{-3}	6.10^{-4}	8.10^{-3}	2.10^{-2}	9.10^{-3}	6.10^{-3}

model seems to fit the experimental data better than those of Toth and Sips. It should be noted that the relative error decreases with temperature in a general way.

Otherwise, from fitting comparison of N_2 and CH_4 adsorption isotherms at 293 K and 253 K respectively (Fig. 9), it can be seen that the models are able to reproduce the experimental data more accurately.
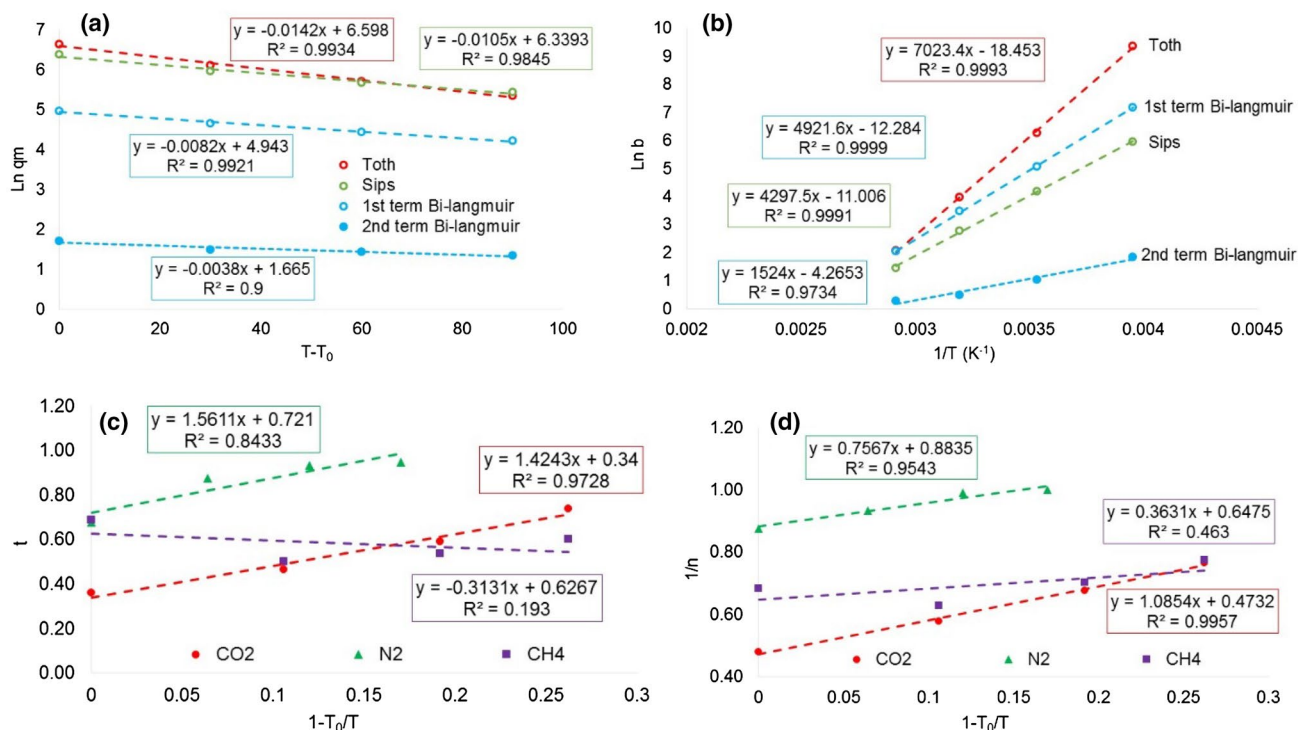
Fig. 11 Evolution of Toth, Sips and Bi-langmuir parameters with temperature on 5A zeolite. **a** CO_2 saturation capacity, **b** CO_2 affinity constant, **c** CO_2, N_2 and CH_4 heterogeneity parameter of Toth model and **d** CO_2, N_2 and CH_4 heterogeneity parameter of Sips model

As cited above, CO_2 adsorption mechanism is controlled by molecule-cation interactions at the lowest pressures and by molecule–molecule-adsorbent interactions at intermediate and high pressures. Some microscopic studies have shown the presence of different cationic sites with a different energy of interaction with CO_2 on LTA zeolites (Montanari and Busca 2008; Zukal et al. 2011; Jaramillo and Chandross 2004; Akten et al. 2003; Martin-Calvo et al. 2014). In this way, the theoretical fundamentals of the classical models evaluated here cannot describe the observed physico-chemical phenomena. This is confirmed by the prediction of the isosteric heat of adsorption at 313 K (Fig. 10). Indeed, none of the models is able to reproduce the experimental isosteric heat of adsorption accurately, even when they accurately represent the adsorption isotherms.

Finally, the fitted model parameters and the value of the objective function are reported in Table 7 at each temperature. The SOR function is notably higher in the case of CO_2 isotherms confirming that classical equilibrium models are not representative of the observed CO_2 adsorption mechanisms on zeolites. In a general way, the variation of the parameters with temperature is consistent with what is expected in the models (for example, Eqs. 13 and 14 for q_m and b). However, in some cases, especially for t and n parameters of the Toth and Sips models, the evolution of

these parameters with temperature is quite random and the theoretical variations (Eqs. 17 and 20) are not recovered (Fig. 11). It confirms that these traditional models, although widely used in the adsorption separation processes, are not sufficiently coherent to faithfully reproduce the experimental data and should not be extrapolated at conditions that were not considered for adjustment.

5 Conclusions

The structural and microscopic properties that control the adsorption mechanisms of CO_2, nitrogen and methane on five zeolites have been identified over a wide range of pressures and temperatures by combining the characterization of the zeolites by gas porosimetry, the measurement of adsorption isotherms by high resolution low-pressure manometry and high pressure gravimetry and the measurement of the adsorption enthalpy with a coupled manometric-calorimetric device. It has been shown that, at these thermodynamic conditions specific of separation or storage processes, CO_2 adsorption is controlled by its interactions with the cations of the zeolites at low pressures and by the pore volume at intermediate and high pressures where cavity filling predominates. On the other hand, nitrogen and methane adsorption mechanism is controlled only by pore volume over the

whole range of operating conditions studied in this work. This new set of experimental data—that covers nearly seven decades of pressure and one hundred degrees—has allowed to assess the classical models which are widely used in the modeling of gas separation processes. It emerges from this study that Toth, Sips and bi-Langmuir models do not allow to describe the physic-chemical phenomena observed in the adsorption of these gases on zeolites. Indeed, they are not able to fit both the experimental adsorption isotherms and heats of adsorption over wide range of pressures and temperatures. Therefore, care must be taken when these models need to be used over thermodynamic conditions that were not considered for the fitting of the parameters.

References

Akten, E.D., Siriwardane, R., Sholl, D.S.: Monte Carlo simulation of single- and binary-component adsorption of CO_2, N_2, and H_2 in zeolite Na-4A. Energy Fuels. **17**, 977–983 (2003). https://doi.org/10.1021/ef0300038

Baerlocher, C., McCusker, L.B., Olson, D.H.: Atlas of Zeolite Framework Types. Elsevier, Amsterdam (2007)

BIPM's: Evaluation of measurement data—Guide to the expression of uncertainty in measurement (2008). https://www.bipm.org/utils/common/documents/jcgm/JCGM_100_2008_E.pdf

Bonenfant, D., Kharoune, M., Niquette, P., Mimeault, M., Hausler, R.: Advances in principal factors influencing carbon dioxide adsorption on zeolites. Sci. Technol. Adv. Mater. **9**, 013007 (2008). https://doi.org/10.1088/1468-6996/9/1/013007

Bourrelly, S., Maurin, G., Llewellyn, P.L.: Adsorption microcalorimetry of methane and carbon dioxide on various zeolites. In: Studies in Surface Science and Catalysis. pp. 1121–1128. Elsevier, Amsterdam (2005)

Cheung, O., Hedin, N.: Zeolites and related sorbents with narrow pores for CO_2 separation from flue gas. RSC Adv. **4**, 14480–14494 (2014). https://doi.org/10.1039/C3RA48052F

Do, D.D.: Adsorption Analysis: Equilibria and Kinetics. Imperial College Press, London (1998)

Dunne, J.A., Mariwala, R., Rao, M., Sircar, S., Gorte, R.J., Myers, A.L.: Calorimetric heats of adsorption and adsorption isotherms. 1. O_2, N_2, Ar, CO_2, CH_4, C_2H_6, and SF6 on silicalite. Langmuir **12**, 5888–5895 (1996a). https://doi.org/10.1021/la960495z

Dunne, J.A., Rao, M., Sircar, S., Gorte, R.J., Myers, A.L.: Calorimetric heats of adsorption and adsorption isotherms. 2. O_2, N_2, Ar, CO_2, CH_4, C_2H_6, and SF6 on NaX, H-ZSM-5, and Na-ZSM-5 Zeolites. Langmuir **12**, 5896–5904 (1996b). https://doi.org/10.1021/la960496r

Gholipour, F., Mofarahi, M.: Adsorption equilibrium of methane and carbon dioxide on zeolite 13X: experimental and thermodynamic modeling. J. Supercrit. Fluids **111**, 47–54 (2016). https://doi.org/10.1016/j.supflu.2016.01.008

Gibbs, J.W. On the equilibrium of heterogeneous substances. Trans. Connecticut Acad. Sci. **1875–1877**(3), 108–248, 343–524 (1877)

Gleichmann, K., Unger, B., Brandt, A.: Industrial zeolite molecular sieves. In: Belviso, C. (ed.) Zeolites—Useful Minerals. InTech, Rijeka (2016)

Harlick, P.J.E., Tezel, F.H.: Adsorption of carbon dioxide, methane and nitrogen: pure and binary mixture adsorption for ZSM-5 with SiO_2/Al_2O_3 ratio of 280. Sep. Purif. Technol. **33**, 199–210 (2003). https://doi.org/10.1016/S1383-5866(02)00078-3

Hefti, M., Marx, D., Joss, L., Mazzotti, M.: Adsorption equilibrium of binary mixtures of carbon dioxide and nitrogen on zeolites ZSM-5 and 13X. Microporous Mesoporous Mater. **215**, 215–228 (2015). https://doi.org/10.1016/j.micromeso.2015.05.044

IZA: Database of Zeolite Structures (2019). https://www.iza-structure.org/databases/

Jaramillo, E., Chandross, M.: Adsorption of small molecules in LTA zeolites. 1. NH_3, CO_2, and H_2O in zeolite 4A. J. Phys. Chem. B. **108**, 20155–20159 (2004). https://doi.org/10.1021/jp048078f

Langmuir, I.: the adsorption of gases on plane surfaces of glass, mica and platinum. J. Am. Chem. Soc. **40**, 1361–1403 (1918). https://doi.org/10.1021/ja02242a004

Llewellyn, P.L., Coulomb, J.P., Grillet, Y., Patarin, J., Lauter, H., Reichert, H., Rouquerol, J.: Adsorption by MFI-type zeolites examined by isothermal microcalorimetry and neutron diffraction. 1. Argon, krypton, and methane. Langmuir **9**, 1846–1851 (1993)

Losch, P.: Synthesis and characterisation of zeolites, their application in catalysis and subsequent rationalisation: methanol-to-olefins (MTO) process with designed ZSM-5 zeolites. PhD Thesis, Universite de Strasbourg (2016)

Lowell, S., Shields, J.E., Thomas, M.A., Thommes, M.: Characterization of Porous Solids and Powders: Surface Area, Pore Size and Density. Springer, Dordrecht (2010)

Martin-Calvo, A., Parra, J.B., Ania, C.O., Calero, S.: Insights on the anomalous adsorption of carbon dioxide in LTA zeolites. J. Phys. Chem. C **118**, 25460–25467 (2014). https://doi.org/10.1021/jp507431c

Maurin, G., Llewellyn, P.L., Bell, R.G.: Adsorption mechanism of carbon dioxide in Faujasites: grand canonical Monte Carlo simulations and microcalorimetry measurements. J. Phys. Chem. B **109**, 16084–16091 (2005). https://doi.org/10.1021/jp052716s

Mofarahi, M., Gholipour, F.: Gas adsorption separation of CO_2/CH_4 system using zeolite 5A. Microporous Mesoporous Mater. **200**, 1–10 (2014). https://doi.org/10.1016/j.micromeso.2014.08.022

Montanari, T., Busca, G.: On the mechanism of adsorption and separation of CO_2 on LTA zeolites: an IR investigation. Vib. Spectrosc. **46**, 45–51 (2008). https://doi.org/10.1016/j.vibspec.2007.09.001

Mouahid, A., Bessieres, D., Plantier, F., Pijaudier-Cabot, G.: A thermostated coupled apparatus for the simultaneous determination of adsorption isotherms and differential enthalpies of adsorption at high pressure and high temperature. J. Therm. Anal. Calorim. **109**, 1077–1087 (2012). https://doi.org/10.1007/s10973-011-1820-2

Newsome, D., Gunawan, S., Baron, G., Denayer, J., Coppens, M.-O.: Adsorption of CO_2 and N_2 in Na–ZSM-5: effects of Na+ and Al content studied by Grand Canonical Monte Carlo simulations and experiments. Adsorption **20**, 157–171 (2014). https://doi.org/10.1007/s10450-013-9560-1

Rouquerol, J., Llewellyn, P., Rouquerol, F.: Is the bet equation applicable to microporous adsorbents? In: Studies in Surface Science and Catalysis, pp. 49–56. Elsevier, Amsterdam (2007)

Ruthven, D.M.: Principles of Adsorption and Adsorption Processes. Wiley, New York (1984)

Sips, R.: Combined form of Langmuir and Freundlich equations. J. Chem. Phys. **16**, 490–495 (1948)

Tagliabue, M., Farrusseng, D., Valencia, S., Aguado, S., Ravon, U., Rizzo, C., Corma, A., Mirodatos, C.: Natural gas treating by selective adsorption: material science and chemical engineering interplay. Chem. Eng. J. **155**, 553–566 (2009). https://doi.org/10.1016/j.cej.2009.09.010

Thommes, M., Mitchell, S., Pérez-Ramírez, J.: Surface and pore structure assessment of hierarchical MFI zeolites by advanced water

and argon sorption studies. J. Phys. Chem. C. **116**, 18816–18823 (2012). https://doi.org/10.1021/jp3051214

Thommes, M., Kaneko, K., Neimark, A.V., Olivier, J.P., Rodriguez-Reinoso, F., Rouquerol, J., Sing, K.S.W.: Physisorption of gases, with special reference to the evaluation of surface area and pore size distribution (IUPAC Technical Report). Pure Appl. Chem. **87**(9–10), 1051–1069 (2015). https://doi.org/10.1515/pac-2014-1117

Toth, J.: State equations of the solid gas interface layer. Acta Chem. Acad. Hung. **69**, 311–317 (1971)

Wang, Y., LeVan, M.D.: Adsorption equilibrium of carbon dioxide and water vapor on zeolites 5A and 13X and silica gel: pure components. J. Chem. Eng. Data **54**, 2839–2844 (2009). https://doi.org/10.1021/je800900a

Wang, J., Huang, L., Yang, R., Zhang, Z., Wu, J., Gao, Y., Wang, Q., O'Hare, D., Zhong, Z.: Recent advances in solid sorbents for CO_2 capture and new development trends. Energy Environ. Sci. **7**, 3478–3518 (2014). https://doi.org/10.1039/C4EE01647E

Wiersum, A.: Developing a strategy to evaluate the potential of new porous materials for the separation of gases by adsorption.

Doctoral thesis in Materials Science, Physics, Chemistry and Nanosciences (2012)

Yang, R.T.: Gas Separation by Adsorption Processes. Imperial College Press, London (1999)

Zimmermann, W., Keller, J.U.: A new calorimeter for simultaneous measurement of isotherms and heats of adsorption. Thermochim. Acta. **405**, 31–41 (2003). https://doi.org/10.1016/S0040-6031(03)00133-3

Zukal, A., Mayerová, J., Kubů, M.: Adsorption of carbon dioxide on high-silica zeolites with different framework topology. Top. Catal. **53**, 1361–1366 (2010). https://doi.org/10.1007/s11244-010-9594-5

Zukal, A., Arean, C.O., Delgado, M.R., Nachtigall, P., Pulido, A., Mayerová, J., Čejka, J.: Combined volumetric, infrared spectroscopic and theoretical investigation of CO_2 adsorption on Na-A zeolite. Microporous Mesoporous Mater. **146**, 97–105 (2011). https://doi.org/10.1016/j.micromeso.2011.03.034